

Supplementary Information

Dinuclear planar chiral ferrocenyl gold(I) & gold(II) complexes

Marta Ayerbe Garcia,^a Wolfgang Frey,^a Mark Ringenberg,^b Max Schwilk,^c and René Peters*^a

Institut für Organische Chemie, Universität Stuttgart, Pfaffenwaldring 55, D-70569 Stuttgart,
Germany^a

^a Universität Stuttgart, Institut für Organische Chemie, Pfaffenwaldring 55, 70569 Stuttgart, Germany. E-mail: rene.peters@oc.uni-stuttgart.de

^b Universität Stuttgart, Institut für Anorganische Chemie, Pfaffenwaldring 55, 70569 Stuttgart, Germany.

^c Universität Stuttgart, Institut für Theoretische Chemie, Pfaffenwaldring 55, 70569 Stuttgart, Germany.

Table of Contents

Experimental.....	2
Synthesis of Dimeric Planar Chiral Ferrocenyl Gold(I) & Gold(II) Complexes.....	3
NMR Spectra of Unknown Compounds.....	7
Electrochemistry	10
Computational Methods and Results.....	13
References.....	25

Experimental

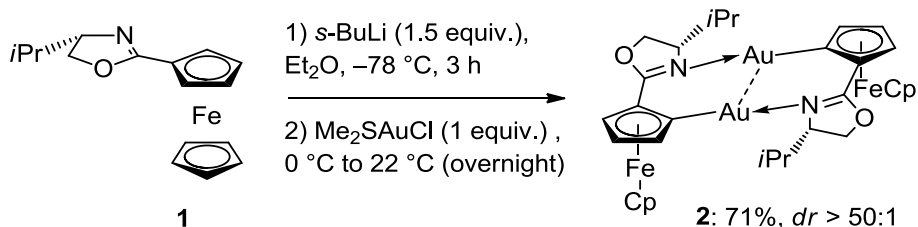
All reactions were performed in oven-dried glassware under a positive pressure of nitrogen and magnetically stirred. Diethylether, THF, toluene, *n*-pentane, acetonitrile and dichloromethane were dried under N₂ over 4Å molecular sieves in a solvent purification system. The solvents petrol ether, chloroform, ethanol, isopropanol, methanol and ethyl acetate were used as purchased from commercial suppliers. Solvents were usually removed at 30–40 °C by rotary evaporation at 600–10 mbar pressure and non-volatile compounds were dried in vacuo at 0.1 mbar. ClAuSMe₂¹ and compound **1**² were prepared according to literature procedures. All other laboratory chemicals were purchased from commercial suppliers and were used without purification unless otherwise indicated. For all reactions liquids were added via syringe. Yields refer to isolated, pure compounds and are calculated in mol% of the used starting material. Reactions were monitored by thin layer chromatography using silica gel 60 F 254 plates (visualization by fluorescence quenching under UV light or staining with cerium ammonium molybdate/sulfuric acid). Column chromatography was carried out on silica gel using distilled technical grade solvents. NMR-spectra were recorded at 21 °C operating at 300 MHz or 500 MHz (¹H) and 125 MHz or 176 MHz (¹³C). Chemical shifts δ are referred in terms of ppm. Abbreviations for multiplicities are as follows: s (singulet), d (doublet), t (triplet), m (multiplet), b (broad signal). IR-spectra were recorded on an ATR unit and the signals are given by wavenumbers (cm⁻¹). Optical rotation was measured in CHCl₃ at the sodium-D-line at 25 °C in a cell with 100 mm path length. Melting points were measured in open glass capillaries and are uncorrected. Mass spectra were measured on an ESI spectrometer by the analytical service of the Institut für Organische Chemie at the Universität Stuttgart. Single crystal X-ray analyses were performed by Dr. Wolfgang Frey (Universität Stuttgart).

Synthesis of Dimeric Planar Chiral Ferrocenyl Gold(I) & Gold(II) Complexes

General Procedure for the Diastereoselective *Ortho*-Functionalization of 1 (GP1)

A solution of oxazoline **1** (1 equiv) in Et₂O (1 mL per 30 mg of **1**) was cooled to -78 °C and was then treated dropwise with *s*-BuLi (1.5 equiv).³ The resulting solution was stirred for 3 h at -78 °C and then warmed to 0 °C and treated with Me₂SAuCl. The reaction mixture was then allowed to slowly warm to room temperature and stirring was continued overnight. The solvent was removed *in vacuo*. The crude product was purified by column chromatography (silica, PE/EtOAc, 80/20).

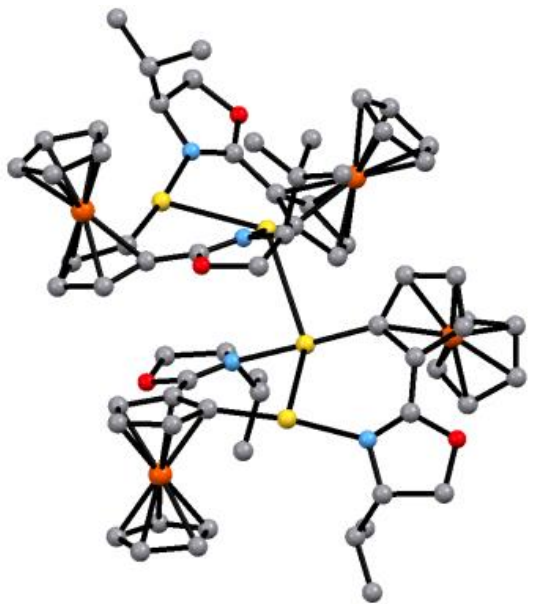
Compound 2



Following **GP1 1** (33.2 mg, 0.110 mmol, 1 equiv.) was treated with *s*-BuLi (1.4 M in hexane, 0.117 mL, 0.165 mmol, 1.5 equiv.) and Me₂SAuCl (32.4 mg, 0.110 mmol, 1 equiv.) to afford **2** (38.5 mg, 0.0391 mmol, 71 %) as a red-orange solid.

$C_{32}H_{36}Au_2Fe_2N_2O_2$, mol wt: 986.265 g/mol. Mp: 154.5-155.3 °C (decomp). $[\alpha]_D^{23} = -1.5$ ($c = 0.7$ g dL $^{-1}$, CHCl $_3$). 1H NMR (300 MHz, CDCl $_3$, 21 °C): δ 4.85 (m, 1 H, H $_{Fc}$), 4.43 (m, 1 H, H $_{Fc}$), 4.35 (m, 3 H, NCHCH $_2$ O), 4.31 (m, 1 H, H $_{Cp}$), 4.16 (s, 5 H, Cp), 2.54 (m, 1 H, CH $_3$ CHCH $_3$), 1.22 (d, $J = 7.3$ Hz, 3 H, CH $_3$ CHCH $_3$), 1.09 (d, $J = 7.3$ Hz, 3 H, CH $_3$ CHCH $_3$). ^{13}C NMR (125 MHz, CDCl $_3$, 21 °C): δ 178.1, 81.9, 81.7, 73.7, 73.4, 72.3, 71.8, 69.8, 68.3, 31.9, 18.4, 15.9. IR (solid): ν 3093, 2955, 2926, 2869, 1741, 1664, 1616, 1477, 1462, 1432, 1376, 1331, 1272, 1229, 1181, 1158, 1134, 1104, 1057, 1032, 999, 977, 955, 885, 805, 626, 599, 560, 518, 481, 449, 421. HRMS (ESI): m/z calcd for [M] $^+$ C $_{32}H_{36}Au_2Fe_2N_2O_2$, 986.0802; found, 986.0822. Anal. calcd for C $_{32}H_{36}Au_2Fe_2N_2O_2$: C, 38.97; H, 3.68; N, 2.84. Found: C, 38.74; H, 3.74; N, 2.45.

A crystal suitable for X-ray analysis could be obtained by slowly evaporating a solution of **2** in *n*-pentane. CCDC 1056862 contains the supplementary crystallographic data for this compound. These data can be obtained free of charge from the Cambridge Crystallographic Data Centre via www.ccdc.cam.ac.uk/data_request/cif.



Compound 3



Method A: A solution of **2** (5.9 mg, 0.0060 mmol, 1 equiv.) in Et_2O (0.2 mL) was cooled to 0 °C and then treated with Me_2SAuCl (3.5 mg, 0.0120 mmol, 2 equiv.). The resulting solution was stirred for 15 min at 0 °C. The solvent was then removed in vacuo. The crude product was purified by column chromatography (silica, PE/EtOAc, 80/20) to yield **3** as a purple solid (4.9 mg, 0.0047 mmol, 78%, *dr* > 50:1).

Method B: A solution of **2** (5.9 mg, 0.0060 mmol, 1 equiv.) in DCM (0.2 mL) was heated in a closed vial to 50 °C and stirred for 5 days at this temperature. The crude product was purified by column chromatography (silica, PE/EtOAc, 80/20) to yield **3** as a purple solid (3.5 mg, 0.0033 mmol, 55%, *dr* > 50:1).

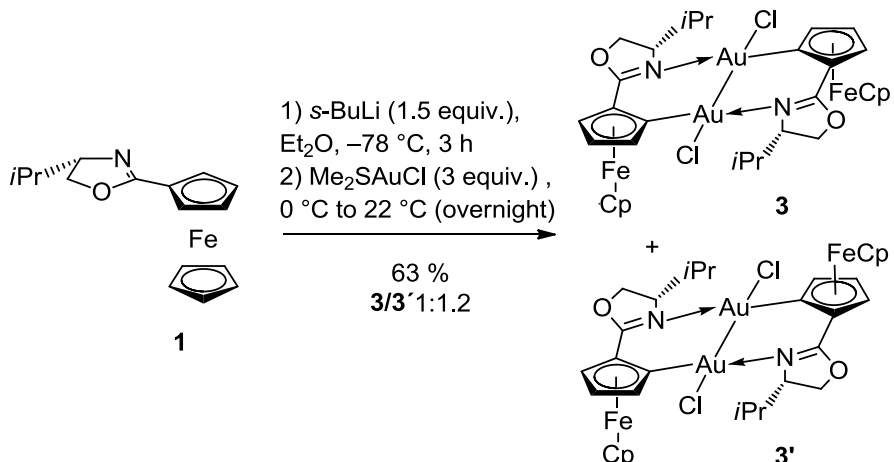
$\text{C}_{32}\text{H}_{36}\text{Au}_2\text{Cl}_2\text{Fe}_2\text{N}_2\text{O}_2$, mol wt: 1057.17 g/mol. Mp: 97.5–98.8 °C (decomp). $[\alpha]_D^{23} = -15.1$ ($c = 0.1$ g dL^{-1} , CHCl_3). ^1H NMR (300 MHz, CDCl_3 , 21 °C): δ 5.13 (m, 1 H, H_{Cp}), 4.77 (m, 2 H, H_{Cp}), 4.59 (m, 2 H, OCH_2), 4.52 (m, 1 H, NCH), 4.31 (s, 5 H, Cp), 2.06 (m, 1 H, CH_3CHCH_3), 1.28 (d, $J = 6.7$ Hz, 3 H, CH_3CHCH_3), 1.19 (d, $J = 6.7$ Hz, 3 H, CH_3CHCH_3). ^{13}C NMR (176 MHz, CDCl_3 , 21 °C): δ 175.8, 81.3, 80.3, 73.0, 72.2, 71.9, 70.6, 70.3, 68.0, 31.7, 18.3, 18.1. IR (solid): ν 2957, 2920, 2850, 1733,

1626, 1485, 1463, 1409, 1374, 1249, 1175, 1154, 1107, 1030, 1000, 973, 912, 879, 822, 731, 510.
 HRMS (ESI): m/z calcd for $[M+nNa]^+$ C₃₂H₃₆Au₂Cl₂Fe₂N₂O₂, 1079.0078; found, 1079.0090.

A crystal suitable for X-ray analysis could be obtained by slowly evaporating a solution of **3** in CH₂Cl₂. CCDC 1056863 contains the supplementary crystallographic data for this compound. These data can be obtained free of charge from the Cambridge Crystallographic Data Centre via www.ccdc.cam.ac.uk/data_request/cif.



Mixture of Compounds **3** and **3'**

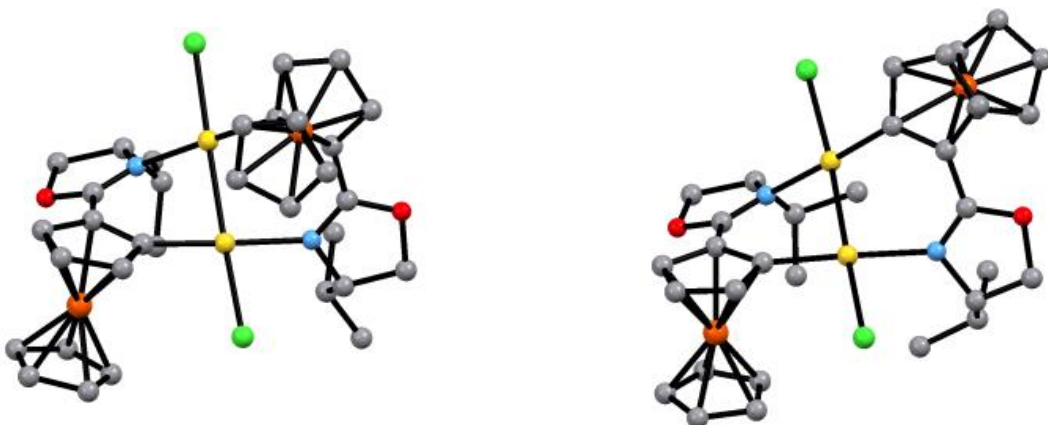


Following **GP1 1** (45.6 mg, 0.151 mmol, 1 equiv.) was treated with *s*-BuLi (1.4 M in hexane, 0.171 mL, 0.227 mmol, 1.5 equiv.) and Me₂SAuCl (0.1334 g, 0.453 mmol, 3 equiv.) to afford a mixture of **3/3'** (1:1.2) as a violet solid (50.3 mg, 0.047 mmol, 63 %).

C₃₂H₃₆Au₂Cl₂Fe₂N₂O₂, mol wt: 1057.17 g/mol. Mp: 98.6-99.3 °C (decomp.). ¹H NMR for compound **3'** (for **3** see above): (300 MHz, CDCl₃, 21 °C): δ 4.93 (m, 1 H, H_{Cp}), 4.81 (m, 1 H, H_{Cp}), 4.71 (m, 1 H, H_{Cp}), 4.64 (m, 1 H, H_{Cp}), 4.60 (m, 2 H, H_{Cp}), 4.53 (m, 2 H, OCH₂), 4.45 (m, 2 H, OCH₂), 4.43 (m, 1 H, NCH), 4.30 (s, 5 H, Cp), 4.29 (s, 5 H, Cp), 4.06 (m, 1 H, NCH), 1.91 (m, 2 H, CH₃CHCH₃), 1.19 (d,

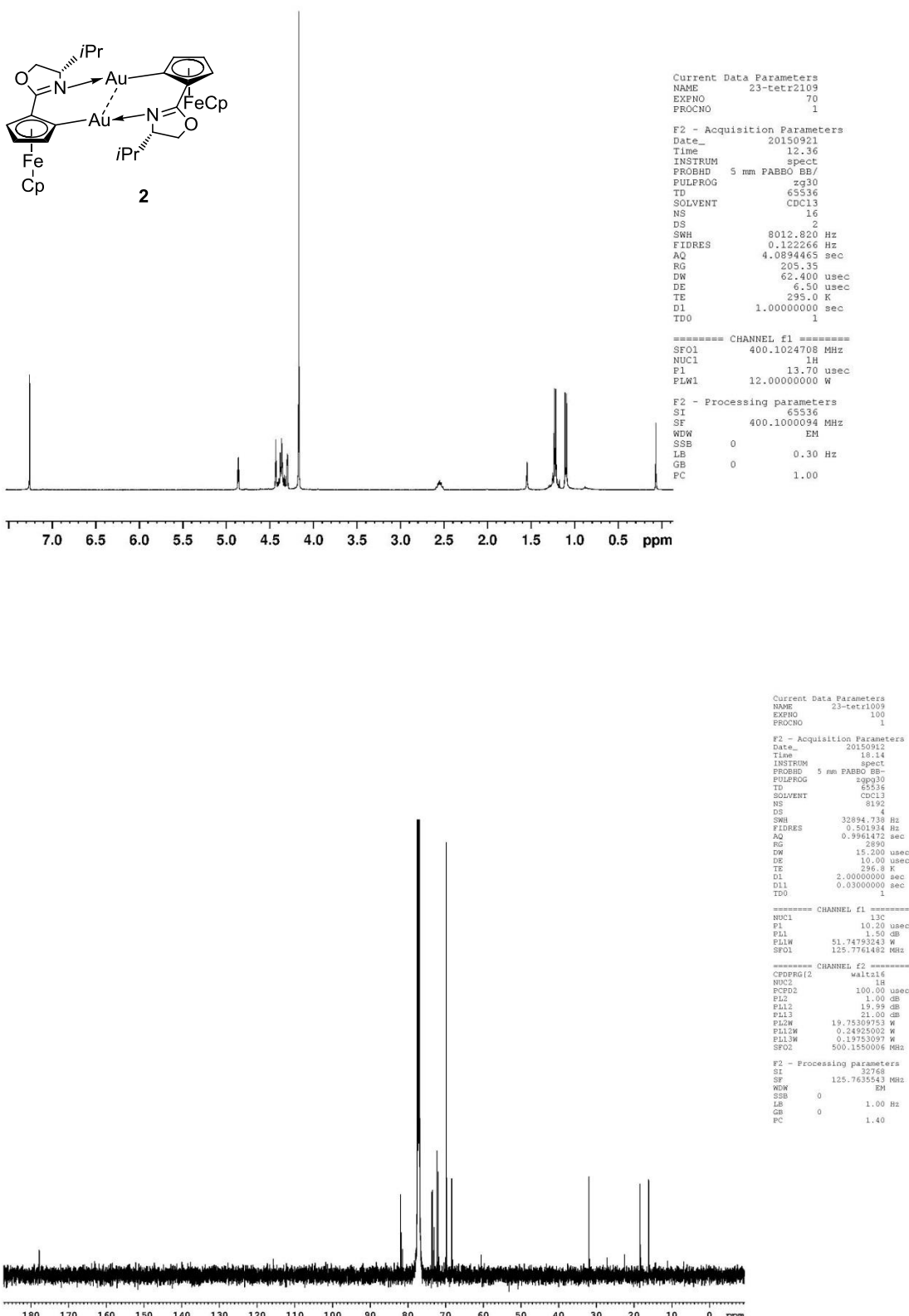
$J = 6.4$ Hz, 3 H, CH_3CHCH_3), 1.05 (d, $J = 6.8$ Hz, 3 H, CH_3CHCH_3), 1.02 (d, $J = 6.4$ Hz, 3 H, CH_3CHCH_3), 0.95 (d, $J = 6.7$ Hz, 3 H, CH_3CHCH_3). ^{13}C NMR (100 MHz, CDCl_3 , 21 °C): δ 177.0, 176.2, 175.7, 81.4, 81.3, 80.3, 73.3, 73.0, 72.5, 72.3, 72.2, 72.17, 72.12, 71.9, 71.2, 71.1, 70.9, 70.67, 70.64, 70.3, 69.6, 68.1, 68.0, 67.4, 32.0, 31.6, 30.8, 29.8, 29.7, 18.6, 18.32, 18.30, 18.2, 18.1, 17.0, 16.5. IR (solid): ν 3095, 2958, 2919, 2871, 2850, 1725, 1624, 1484, 1460, 1410, 1384, 1374, 1331, 1280, 1248, 1175, 1154, 1106, 1060, 1031, 1000, 973, 950, 911, 879, 822, 730, 646, 624, 598, 559, 506. HRMS (ESI): m/z calcd for $[\text{M}-\text{Cl}]^+$ $\text{C}_{32}\text{H}_{36}\text{Au}_2\text{ClFe}_2\text{N}_2\text{O}_2$, 1021.0491; found, 1021.0485.

A crystal of **3'** suitable for X-ray analysis could be obtained by slowly evaporating a solution of **3** and **3'** in $\text{CH}_2\text{Cl}_2/n$ -pentane. CCDC 1056865 contains the supplementary crystallographic data for this compound. These data can be obtained free of charge from the Cambridge Crystallographic Data Centre via www.ccdc.cam.ac.uk/data_request/cif.

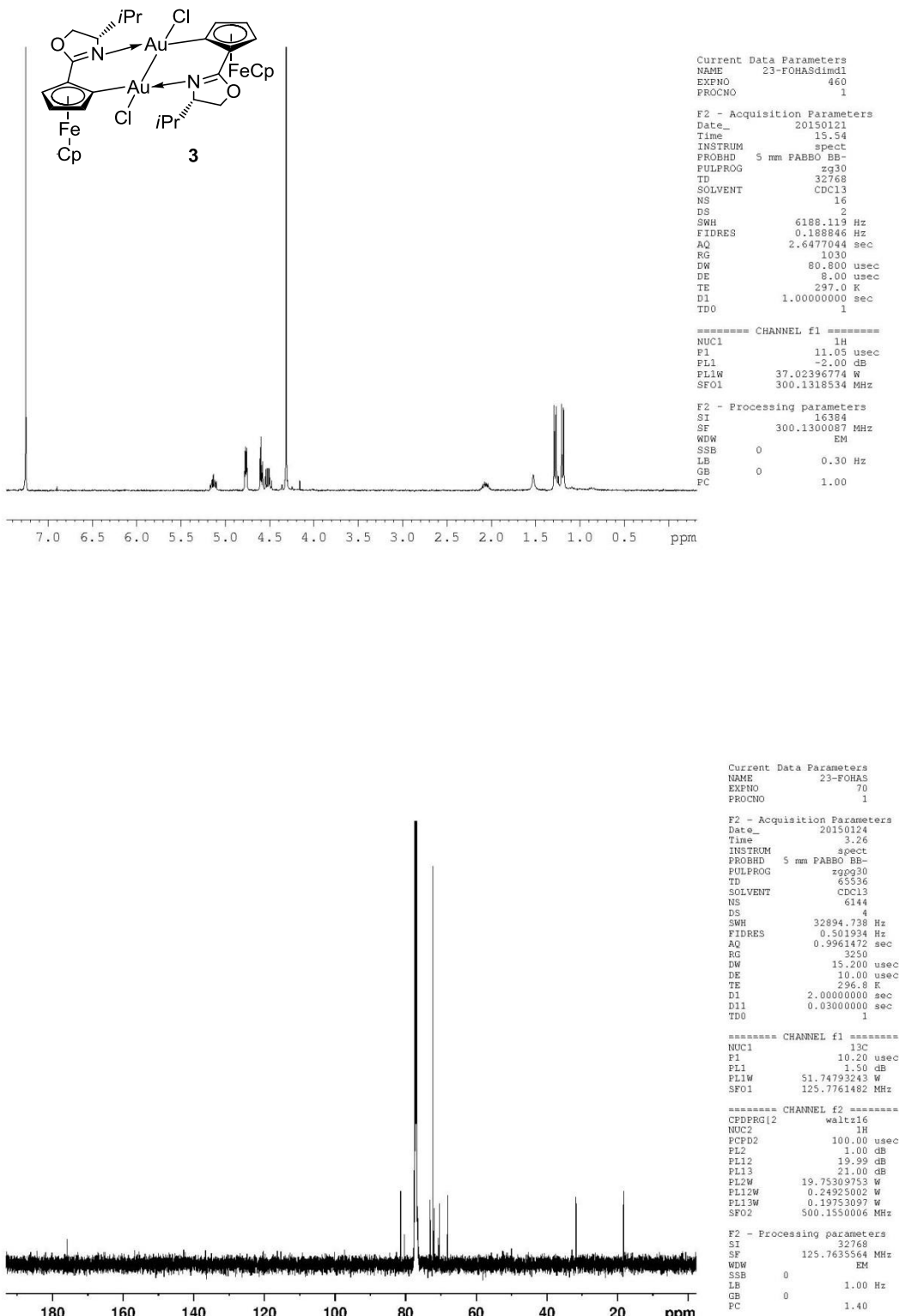


NMR Spectra of Unknown Compounds

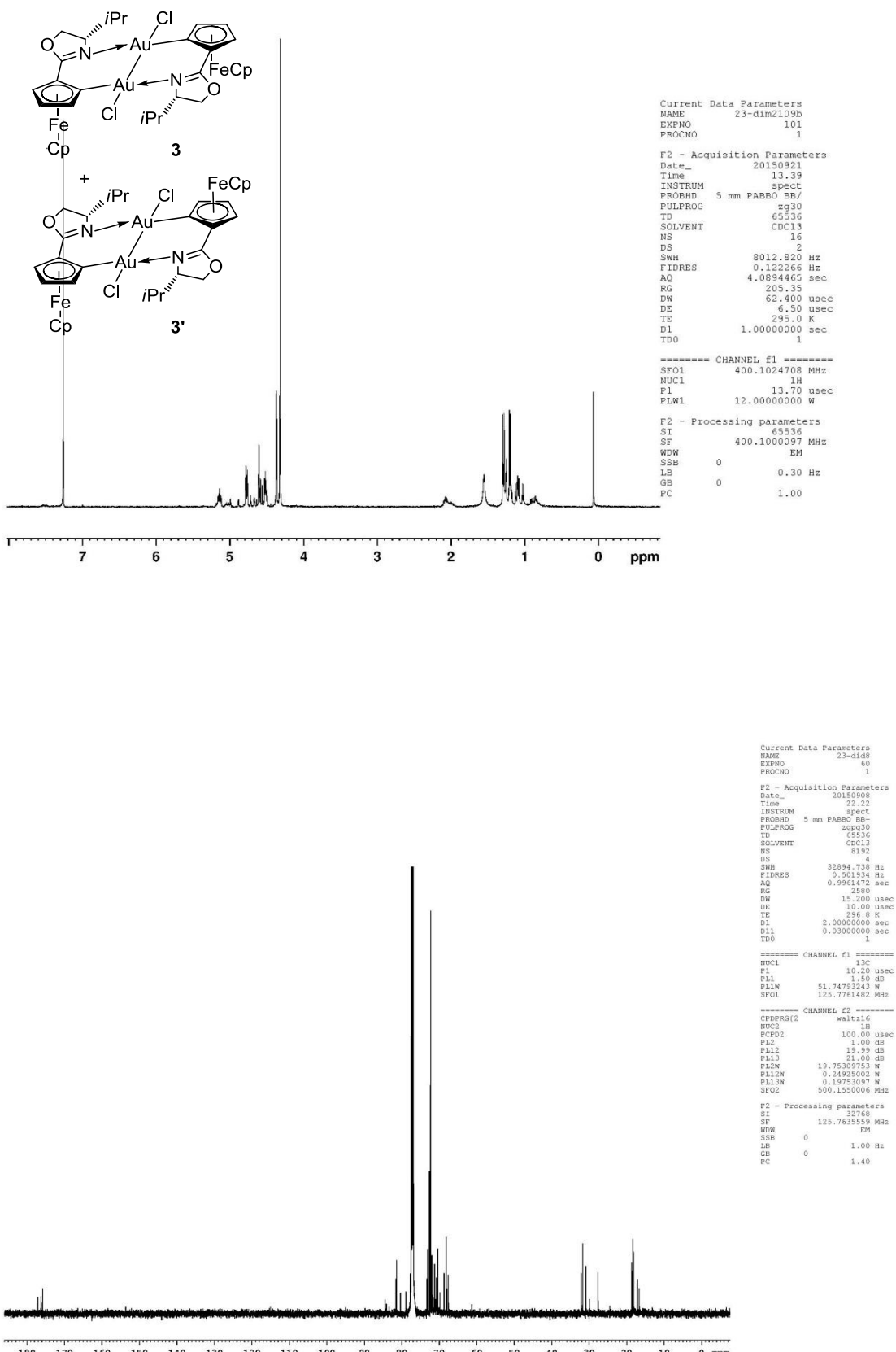
Compound 2



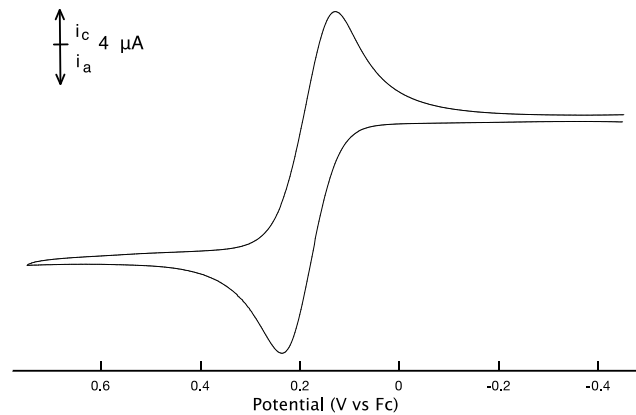
Compound 3



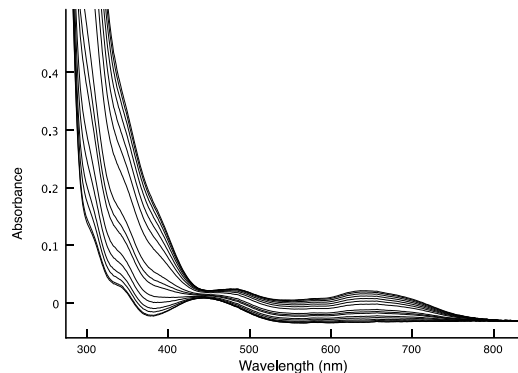
Mixture of 3 and 3' (1:2)



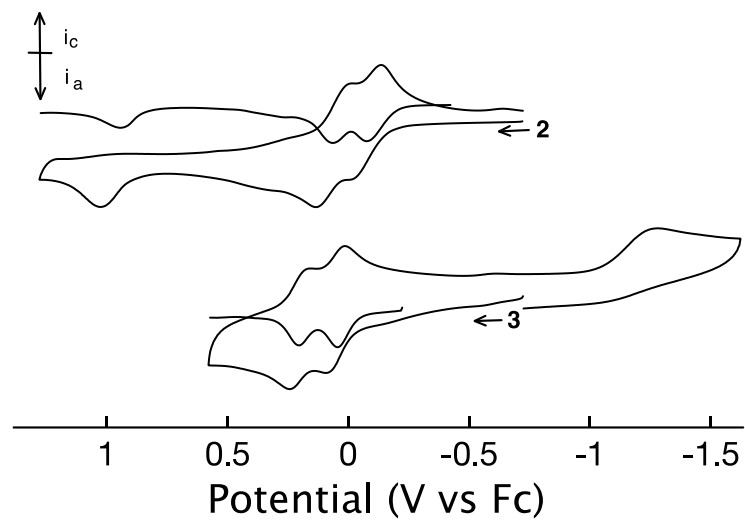
Electrochemistry



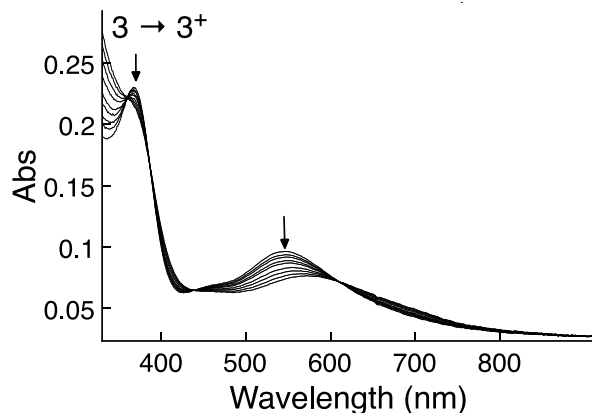
Cyclic voltammogram at 100 mV/s of ligand in CH_2Cl_2 with 0.1 M Bu_4NPF_6 of supporting electrolyte referenced versus $\text{Fc}^{(0/\text{I})}$.



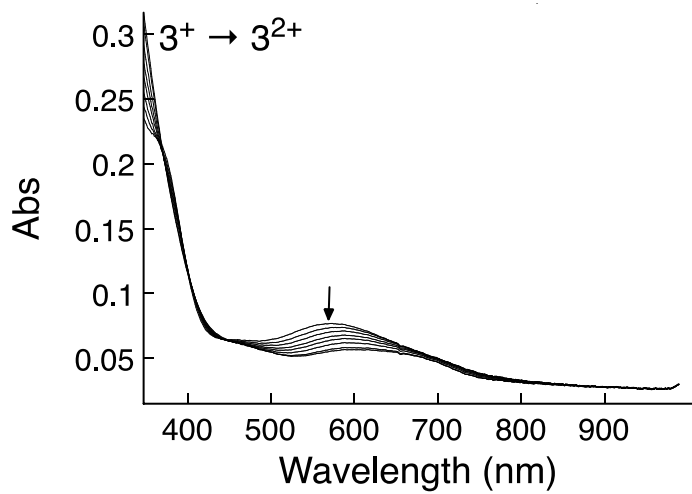
UV-Vis-NIR SEC of **3** in CH_2Cl_2 with 0.1 M Bu_4NPF_6 of supporting electrolyte. Ag/Ag^+ reference, Pt mesh working and Pt counter electrode.



Cyclic voltammogram at 100 mV/s of **7**, and **8** in CH_2Cl_2 with 0.1 M Bu_4NPF_6 of supporting electrolyte referenced versus $\text{Fc}^{(0/\text{I})}$.



UV-Vis-NIR SEC of **8** in CH_2Cl_2 with 0.1 M Bu_4NPF_6 of supporting electrolyte. Ag/Ag^+ reference, Pt mesh working and Pt counter electrode.



UV-Vis-NIR SEC of **8** in CH_2Cl_2 with 0.1 M Bu_4NPF_6 of supporting electrolyte. Ag/Ag^+ reference, Pt mesh working and Pt counter electrode.

Computational Methods and Results

The nonempirical meta-GGA functional TPSS⁴ was chosen within the Kohn-Sham Density Functional Theory for the geometry optimization since in combination with Grimme's D3 dispersion correction⁵ it reliably yields optimized energy minimum structures for closed shell transition metal complexes within the accuracy needed for this study⁶ in combination a triple zeta basis.⁷ Other functionals tested were the hybrid-meta-GGA functional TPSSH,⁴ as well as the nonempirical GGA functional PBE⁸ and its hybrid counterpart PBE0,⁸ all frequently used in DFT studies of gold organometallic compounds.^{6,7,9} The double hybrid functional B2PLYP¹⁰ was shown to yield particular good energy values for gold complexes,^{9,11} however the MP2 correlation energy contribution, which is added separately from the SCF cycle, does not contribute to a better description of the single determinant wavefunction, on which the analysis of the Kohn-Sham¹² and Intrinsic Bond Orbitals (IBOs)¹³ is based. The crystal structure of (Me₂S)Au was taken from Jones and Lautner.¹⁴ The crystal structures were preoptimized using the def2-TZVP¹⁵ basis set with RI-DFT in combination with the MARI-J approximation¹⁶ in TURBOMOLE.¹⁷ For the density fitting the def2-TZVP basis was chosen with a m3 grid and an energy convergence criteria of 10⁻⁷ Hartree in the SCF cycles, using the default energy minimum search algorithm in TURBOMOLE. Numerical second derivatives were calculated to confirm that minimum structures were obtained. In the following, the structures were further optimized using the m4 grid with the def2-TZVP basis in combination with a def2-QZVP density fitting basis and a convergence energy criteria of 10⁻⁸ Hartree in the SCF cycles, while the cartesian gradient norm convergence threshold was set to 10⁻⁴ (in atomic units) and mass weighted derivatives were used. All other parameters were left as for the geometry preoptimization. The approximate Hessian contained only positive eigenvalues, confirming the energy minimum. Diethylether was chosen as solvent in COSMO¹⁸ (relative dielectric permittivity $\epsilon=4.24$), for the refraction index and the atomic radii in the cavity construction, the default values for COSMO within TURBOMOLE were used, since it can be assumed that minor modifications of these values do not have a significant influence on the results. For the gold atom an effective core potential for the inner 60 atoms¹⁹ was used for the accounting of scalar-relativistic effects. The optimized structures are given in Cartesian coordinates in the Tables 3, 4, and 5. The shapes of the Kohn-Sham orbitals are depicted in Figure 1 (for the orbital visualization the Chimera visualization software²⁰ was used), they show very similar or virtually equal shapes for all functionals in the same relative energetic ordering, even though their absolute values diverge quite significantly, as can be seen from Table 6. Similar to findings for simpler dinuclear Au(I) compounds,²¹ the highest occupied Kohn-Sham orbitals that are located on the gold atoms bear σ^* and δ^* Au-Au bonds. Moreover, the finding that no prevalent oxidation center can be determined emerges for all functionals. Interpretation of the electronic structure in terms of closed-shell Kohn-Sham orbitals for ferrocene moieties is common²² since the singlet character of the ground state is a reasonable approximation.²³ IBOs were calculated in MOLPRO²⁴ using the def2-TZVP basis

set with the def2-QZVP basis set for density fitting and the default grid for an energy convergence threshold of 10^{-8} Hartree, using the TPPS, TPPSH, PBE, and the PBE0 functionals. The exponents 2 and 4 in the localization functional of the IBO localization were both tested. For the valence orbitals of the gold centers of the structures **2** and **3**, the charges located on all significantly implicated centers are given in Table 1 and Table 2 for all combinations of functionals and IBO localization exponents (IBOs that are pairwise equivalent by symmetry are only listed once). It gets clear from these results that the qualitative deductions of the IBO analysis are independent from the functional. The differences in bond charge repartitions for varying IBO localization functional exponents (2 or 4) seem qualitatively quite different for the Au-C and the Au-Cl bonds in **3**, but bear the same interpretation: An IBO localization coefficient of 4 enforces a symmetry breaking of the IBOs (similar issues have already been pointed out e. g. for the benzene molecule¹³) which we here do not consider useful for the interpretation in terms of Lewis structures (e. g. the symmetry of the Au-Au bond also breaks down). But, most importantly, the significant +M effect from the Cl-Au bond onto the remote Au atom, does not vanish in the case of an exponent of 4, but is just excessively expressed for one of the two Cl-Au bonds, while being almost completely suppressed for the other. Hence, the +M effect as such does not get suppressed by the more aggressive localization exponent of 4, since it is intrinsically linked to the interpretation of the orbitals in terms of Lewis structures. We note that there is also a very minor +M effect of the C-Au bond onto the remote Au atom in **3**. In **2**, since there is no covalent communication between the two Au centers, both IBO localization functional exponent choices lead to virtually the same bond charge repartition. IBOs of the calculations using the TPSS functional with the localization functional exponent 2 are shown in Figures 2 and 3 except for the Au-Au and the Au-Cl bonds of **3**, which are already depicted in the main text (also, one inert Au lone pair of **2** is not depicted). For the structures **2** and **3**, the π -back-donation of the Au atom to the C atom is weak (part of the bond located on the Au atom of the two d-orbital lone pairs in question: 97%/98% and 98%/99% in **2** and **3** respectively). This is a common finding in the context of other gold complexes,^{6,25} but clearly correlates with the dative bond strength, as already shown for gold carbene complexes.⁶ Curiously, we also observe a very weak, yet noticeable σ -backbonding from the lone pair on the Au atom that mainly consists of a d_{z^2} -orbital towards the C atom (see Figure 2, middle image). Concerning the bonds depicted in Figure 4 of the main text, a d_{z^2} -orbital lone pair obtained by the IBO analysis with a z-axis orthogonal to the plane of the Au bonds permits to interpret the d-orbital contributions to the Au-Au and Au-Cl bonds as stemming from $d_{x^2-y^2}$ orbitals. The IBOs elucidate also the mesomeric stabilization of the Au-C and Au-N bonds by the ligand moieties both in **2** and **3**. In the context of gold complexes, orbital localization and energy decomposition methods have been used extensively,^{7,9,26} equally concluding that bimetallic Au(I) complexes do not form covalent bonds in the ground state.^{21,27}

Figure 1: Kohn-Sham orbitals HOMO to HOMO-6 for **2** for the different functionals used.

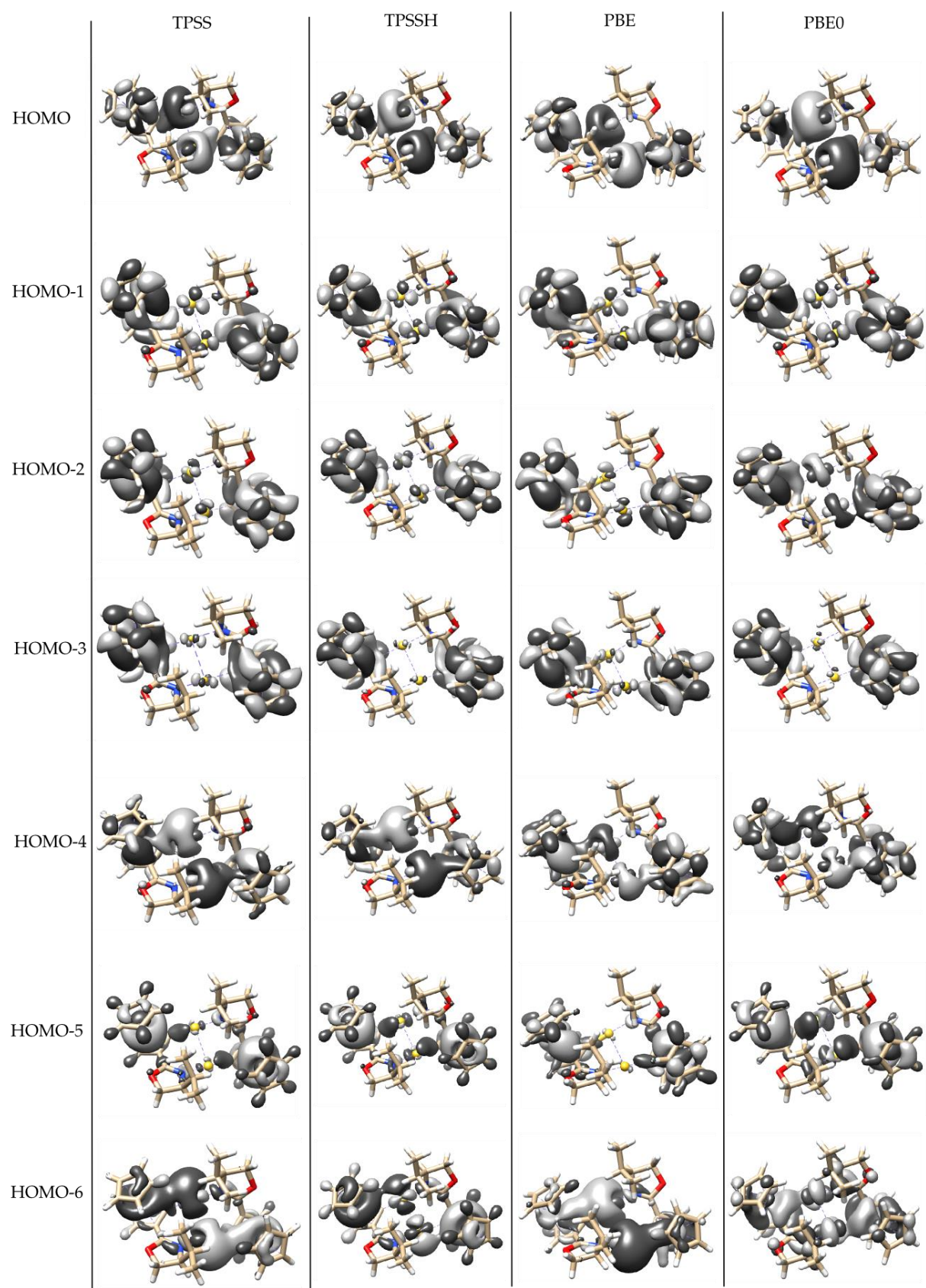


Figure 2: IBOs involving gold atoms in **2** (the iso-surface encloses 85% of the electron density, visualization realised with IboView²⁸).

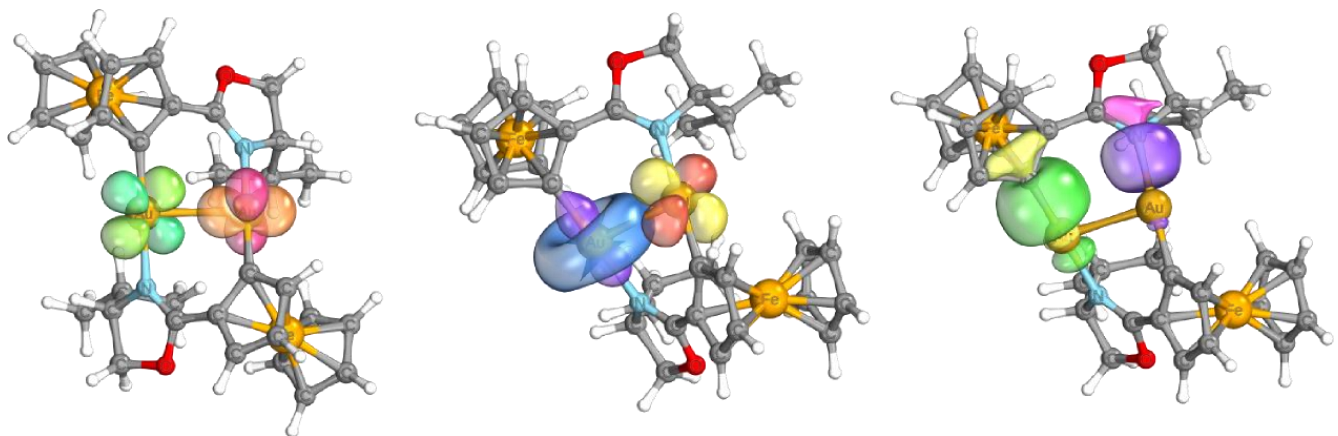


Figure 3: IBOs involving gold atoms in **3** (the iso-surface encloses 85% of the electron density, visualization realised with IboView).

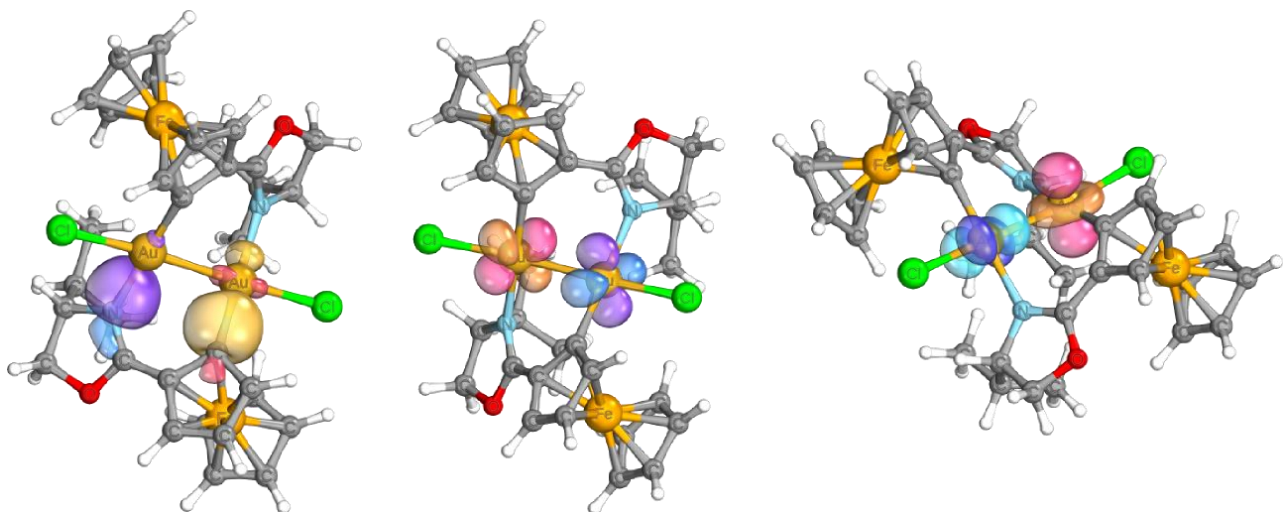


Table 1: IBO bond charge partition for **2**: Bold letters denote the functional (first column) and the IBO localization functional exponent (second column). Each line in normal text describes the charge repartition of one IBO, giving first the atomic center, then its part of the bond charge.

PBE0 2									
N	1.692	Au1	0.222	C1	0.038	C2	0.022	other	0.025
C1	1.389	Au1	0.564	other	0.047				
Au1	1.981								
Au1	1.954	C1	0.022	other	0.024				
Au1	1.966	other	0.034						
Au1	1.997								
Au1	1.998								
PBE0 4									
N	1.693	Au1	0.22	C1	0.037	C2	0.023	other	0.027
C1	1.392	Au1	0.558	other	0.05				
Au1	1.997								
Au1	1.981								
Au1	1.954	other	0.046						
Au1	1.967	other	0.033						
Au1	1.998								
PBE 2									
N	1.674	Au1	0.229	C1	0.045	C2	0.024	other	0.028
C1	1.353	Au1	0.598	other	0.048				
Au1	1.978	other	0.022						
Au1	1.944	C1	0.027	other	0.029				
Au1	1.958	other	0.042						
Au1	1.996								
Au1	1.997								
PBE 4									
N	1.676	Au1	0.227	C1	0.044	C2	0.025	other	0.029
C1	1.358	Au1	0.591	other	0.052				
Au1	1.978	other	0.022						
Au1	1.997								
Au1	1.943	C1	0.023	other	0.034				
Au1	1.96	other	0.04						
Au1	1.996								
TPSS 2									
N	1.681	Au1	0.227	C1	0.042	C2	0.024	other	0.027
C1	1.368	Au1	0.584	other	0.048				
Au1	1.979	other	0.021						
Au1	1.945	C1	0.026	other	0.029				
Au1	1.959	other	0.041						
Au1	1.997								
Au1	1.997								
TPSS 4									
N	1.683	Au1	0.224	C1	0.041	C2	0.024	other	0.029

C1	1.372	Au1	0.576	other	0.051				
Au1	1.979	other	0.021						
Au1	1.944	C1	0.022	other	0.033				
Au1	1.961	other	0.039						
Au1	1.997								
Au1	1.997								
TPSSH 2									
N	1.687	Au1	0.224	C1	0.04	C2	0.023	other	0.026
C1	1.381	Au1	0.571	other	0.048				
Au1	1.98								
Au1	1.949	C1	0.024	other	0.027				
Au1	1.962	other	0.038						
Au1	1.997								
Au1	1.998								
TPSSH 4									
N	1.689	Au1	0.221	C1	0.039	C2	0.024	other	0.028
C1	1.385	Au1	0.565	other	0.051				
Au1	1.98								
Au1	1.949	C1	0.021	other	0.03				
Au1	1.964	other	0.036						
Au1	1.997								
Au1	1.998								

Table 2: IBO bond charge partition for **3**: Bold letters denote the functional (first column) and the IBO localization functional exponent (second column). Each line in normal text describes the charge repartition of one IBO, giving first the atomic center, then its part of the bond charge.

PBE0 2									
Au1	0.988	Au2	0.985	other	0.027				
Au1	1.971	other	0.029						
Au1	1.979	other	0.021						
Au1	1.996								
Au1	1.998								
C1	1.194	Au2	0.735	Au1	0.039	other	0.032		
C11	1.68	Au1	0.149	Au2	0.133	other	0.038		
N	1.68	Au1	0.195	C2	0.072	C3	0.022	other	0.031
PBE0 4									
Au1	1.971	other	0.029						
Au1	1.979	other	0.021						
Au1	1.995								
Au1	1.998								
Au2	1.297	Au1	0.609	C2	0.031	C1	0.03	other	0.032
C1	1.172	Au2	0.59	Au1	0.193	other	0.045		
C2	1.148	Au1	0.814	other	0.038				
C11	1.673	Au1	0.207	Au2	0.072	other	0.048		
Cl2	1.673	Au1	0.183	Au2	0.092	other	0.052		

N	1.686	Au1	0.177	C2	0.079	C3	0.024	other	0.033
PBE 2									
Au1	0.989	Au2	0.982	other	0.029				
Au1	1.963	other	0.037						
Au1	1.973	other	0.027						
Au1	1.994								
Au1	1.998								
C1	1.17	Au2	0.76	Au1	0.037	other	0.033		
Cl1	1.659	Au1	0.156	Au2	0.14	other	0.044		
N	1.665	Au1	0.198	C2	0.08	C3	0.024	other	0.034
PBE 4									
Au1	1.964	other	0.036						
Au1	1.974	other	0.026						
Au1	1.995								
Au1	1.996								
Au2	1.376	Au1	0.491	C1	0.049	C2	0.038	other	0.046
C1	1.123	Au2	0.587	Au1	0.238	other	0.052		
C2	1.089	Au1	0.881	other	0.03				
Cl1	1.647	Au1	0.23	Au2	0.063	other	0.061		
Cl2	1.648	Au1	0.201	Au2	0.085	C2	0.023	other	0.043
N	1.672	Au1	0.172	C2	0.093	C3	0.026	other	0.037
TPSS 2									
Au1	0.988	Au2	0.984	other	0.027				
Au1	1.965	other	0.035						
Au1	1.974	other	0.026						
Au1	1.995								
Au1	1.998								
C1	1.186	Au2	0.743	Au1	0.037	other	0.034		
Cl1	1.667	Au1	0.154	Au2	0.137	other	0.042		
N	1.671	Au1	0.198	C2	0.075	C3	0.023	other	0.033
TPSS 4									
Au1	1.965	other	0.035						
Au1	1.975	other	0.025						
Au1	1.994								
Au1	1.998								
Au2	1.343	Au1	0.544	C1	0.039	C2	0.033	other	0.041
C1	1.152	Au2	0.585	Au1	0.213	other	0.049		
C2	1.128	Au1	0.837	other	0.035				
Cl1	1.657	Au1	0.222	Au2	0.066	other	0.055		
Cl2	1.658	Au1	0.196	Au2	0.087	other	0.06		
N	1.678	Au1	0.177	C2	0.084	C3	0.026	other	0.036
TPSSH 2									
Au1	0.988	Au2	0.985	other	0.027				
Au1	1.968	other	0.032						
Au1	1.977	other	0.023						
Au1	1.995								

Au1	1.998								
C1	1.193	Au2	0.736	Au1	0.038	other	0.033		
Cl1	1.674	Au1	0.151	Au2	0.135	other	0.04		
N	1.677	Au1	0.196	C2	0.073	C3	0.022	other	0.032
TPSSH									4
Au1	1.314	Au2	0.587	C2	0.033	C1	0.031	other	0.036
Au1	1.968	other	0.032						
Au1	1.977	other	0.023						
Au1	1.995								
Au1	1.998								
C1	1.146	Au2	0.817	other	0.038				
C2	1.169	Au1	0.587	Au2	0.198	other	0.047		
Cl1	1.667	Au2	0.189	Au1	0.09	other	0.055		
Cl2	1.666	Au2	0.214	Au1	0.07	other	0.051		
N	1.679	Au1	0.18	C2	0.071	C3	0.025	other	0.044

Table 3: Cartesian coordinates of the optimized structure of **2** in Angstrom.

C	-2.914824	12.8268068	29.9419941
N	-1.6995062	12.7618276	30.7923508
C	-1.0515434	13.8857843	30.6860882
O	-1.5334839	14.7407996	29.7471861
C	-2.6298238	14.0549513	29.0608538
Au	-1.3762692	11.0829116	31.9967637
C	-1.1144554	9.4624124	33.1447642
C	-1.3316443	9.3487084	34.5816441
C	-1.1549879	7.9688951	34.9882098
C	-0.7964679	7.2279406	33.8245029
C	-0.7835033	8.1311898	32.7123338
Fe	-2.6200826	8.121059	33.6093392
C	-3.9472625	7.6499071	32.137236
C	-4.3254235	8.8758216	32.7740116
C	-4.523233	8.6061006	34.1671295
C	-4.2762574	7.214477	34.3924393
C	-3.919592	6.6217296	33.1368393
C	-1.7430309	10.3843929	35.5090697
O	-2.4422354	9.9630684	36.5947086
C	-2.6652228	11.1321861	37.4465901
C	-2.2677626	12.3255814	36.5605807
N	-1.5222484	11.6661757	35.458755
Au	-0.4723858	12.8405778	34.0812473
C	0.5111259	14.0003203	32.7778988
C	0.1164164	14.3384337	31.4160657
C	1.0483035	15.3046372	30.8699894
C	2.0389347	15.5460434	31.86612
C	1.7047551	14.7651648	33.0199688
C	-3.4347865	13.1662501	35.9934026
C	-4.1287986	13.9483669	37.1161033

Fe	0.1720793	16.0279251	32.5370506
C	-0.1734747	17.1311386	34.2143896
C	-1.3814149	16.4961205	33.7797235
C	-1.6548143	16.9365925	32.4441413
C	-0.6230509	17.8484444	32.054004
C	0.2942651	17.9696431	33.1489616
C	-4.183593	12.9047173	30.8224145
C	-4.1813859	14.1247314	31.7508164
C	-4.4254656	12.3246443	35.1806273
C	-5.4455819	12.8446037	29.9520326
H	-1.2613578	7.5894025	35.9955089
H	-0.6068066	6.162531	33.7876197
H	-0.5980491	7.8466191	31.6846908
H	-4.3940253	9.843567	32.296436
H	-4.7695829	9.3337293	34.9280295
H	-4.3186974	6.7077895	35.3477265
H	-3.6458191	5.5869783	32.9763154
H	-3.6927011	7.5290454	31.09247
H	-2.0285575	11.025374	38.3286323
H	-3.7159491	11.1189971	37.7421755
H	-1.5829178	12.9942042	37.0902286
H	-2.9638367	13.8848336	35.3076628
H	-4.9356952	11.5879581	35.8129158
H	-3.9169239	11.7947779	34.3683179
H	-5.1937867	12.9672148	34.7392156
H	-4.9015711	14.6049923	36.7029635
H	-3.4137528	14.5682403	37.6691895
H	-4.6163392	13.2723445	37.8295972
H	0.9987126	15.7397246	29.8809384
H	2.8727608	16.2307794	31.774896
H	2.2447846	14.7825029	33.9578051
H	-1.9543602	15.7713389	34.3416126
H	-2.4724624	16.6053733	31.8190236
H	-0.5339372	18.3332696	31.0906869
H	1.1985652	18.564351	33.1590977
H	0.3180087	16.9776704	35.1661363
H	-2.2790555	13.7889098	28.0602972
H	-3.4575739	14.7627683	28.9894498
H	-2.9649788	11.9159755	29.3383884
H	-4.1516117	12.0043766	31.452293
H	-5.5234635	13.7252149	29.3023068
H	-6.3418387	12.8178836	30.5805634
H	-5.4473598	11.9517014	29.3163062
H	-3.2905331	14.1320209	32.3877354
H	-5.0631327	14.107449	32.398943
H	-4.2107903	15.0604775	31.1795772

Table 4: Cartesian coordinates of the optimized structure of **3** in Angstrom.

C	11.8531019	18.2093696	6.7008205
N	11.3455918	16.8161693	6.6054419
C	12.3463676	15.9917133	6.6935625
O	13.5691532	16.5570289	6.7489918
C	13.3703667	18.0010318	6.5432971
Au	9.4112049	16.2278728	5.9627211
Au	9.2873766	14.373998	7.7539651
C	11.1074226	13.7687751	7.1184407
C	12.2616567	14.5537141	6.7138085
C	13.3495654	13.6559411	6.4033891
C	12.8652704	12.3266357	6.5817046
C	11.5047883	12.3936479	7.0215657
Fe	12.7155143	13.4174052	8.3107478
C	14.3667934	13.6639266	9.4928318
C	13.3658847	14.631476	9.8240801
C	12.1796049	13.931838	10.2162376
C	12.4453596	12.5281716	10.1256732
C	13.7976062	12.3618486	9.6812171
C	11.4255588	18.895447	8.0164243
C	9.9118903	19.140298	8.0311882
Cl	9.6625124	17.8388465	4.1366299
C	7.5958888	15.6060578	5.3298494
C	6.4402332	15.1706403	6.0960941
C	5.3573179	14.8858439	5.184
C	5.8461696	15.1103876	3.8634067
C	7.2044226	15.5535032	3.9506822
Fe	5.984064	16.8026722	5.0118595
C	4.3264128	17.9693043	5.2889866
C	5.320673	18.2718187	6.2726255
C	6.5091939	18.6918283	5.5931612
C	6.2513087	18.6476588	4.1858187
C	4.9018537	18.2037465	3.9972135
C	6.3504337	15.1018621	7.5322814
O	5.1256946	15.1336972	8.0952929
C	5.32122	14.8800176	9.5322432
C	6.8368039	15.0390344	9.7504888
N	7.348948	14.9900473	8.3565976
C	7.2555404	16.3349898	10.4781927
C	6.7940488	17.5959148	9.7369419
C	8.7694193	16.3529616	10.7213873
Cl	9.0367781	12.4925097	9.2993955
C	11.878463	18.1138438	9.255851
H	7.8271753	15.8607603	3.1226756
H	5.2691332	15.008773	2.9533384
H	4.3660652	14.5579491	5.4657166
H	5.2033438	18.1569974	7.3411891
H	7.4558338	18.9451479	6.0493807

H	6.9724799	18.8601108	3.4095006
H	4.4147178	18.0386665	3.0451112
H	3.3295005	17.5976241	5.4861047
H	4.9657958	13.8659208	9.7302836
H	4.7133702	15.6067137	10.0732547
H	7.2457417	14.1790242	10.285714
H	6.7513637	16.2947493	11.4545934
H	5.7031008	17.6394125	9.6456754
H	7.2235395	17.6260212	8.7301427
H	7.1199683	18.4951062	10.2690703
H	9.310313	16.406559	9.7702462
H	9.0965152	15.4488305	11.2460544
H	9.0572984	17.2260994	11.3159489
H	10.8843741	11.5533357	7.2985889
H	13.4465587	11.4227968	6.4525947
H	14.3410316	13.9525062	6.0895556
H	13.4775538	15.7039145	9.7455801
H	11.2295697	14.3741245	10.4810457
H	11.7275884	11.7413106	10.3089821
H	14.2906822	11.418502	9.4861429
H	15.3640216	13.8788613	9.1320236
H	13.7311387	18.2346781	5.5387244
H	13.9722018	18.5188168	7.29162
H	11.4469	18.7698422	5.8557493
H	11.9306528	19.8721875	8.010893
H	12.9692359	18.0225505	9.3042137
H	11.4503612	17.1060241	9.2499975
H	11.5453035	18.6159086	10.1695463
H	9.3683758	18.1891399	8.0440071
H	9.5936193	19.699197	7.1445596
H	9.617771	19.7025256	8.9234497

Table 5: Cartesian coordinates of the optimized structure of (Me₂S)Au in Angstrom.

Au	0.0324369	-0.0698123	0.0217591
S	0.1721022	0.0114444	2.2979469
Cl	-0.049722	-0.1483962	-2.2610185
C	-0.8820945	1.4020406	2.8336136
C	-0.8115398	-1.3901911	2.9302595
H	-0.2987072	-2.3008126	2.6178066
H	-1.8209069	-1.3599965	2.5187758
H	-0.8266854	-1.3195056	4.020224
H	-0.8956712	1.4061254	3.9258595
H	-0.415314	2.3135745	2.458039
H	-1.8879089	1.2925614	2.4268858

Table 6: Orbital energies of selected occupied Kohn-Sham orbitals of **2** for the different functionals (in eV).

Orbital	TPSS	TPSSH	PBE	PBE0
HOMO	-4.12	-4.66	-4.12	-5.42
HOMO-1	-4.25	-4.86	-4.27	-5.85
HOMO-2	-4.30	-4.90	-4.33	-5.86
HOMO-3	-4.33	-4.91	-4.35	-5.90
HOMO-4	-4.47	-5.03	-4.40	-5.92
HOMO-5	-4.59	-5.42	-4.43	-6.56
HOMO-6	-4.81	-5.54	-4.76	-6.64

References

- ¹ T. E. Müller, J. C. Green, D. M. P. Mingos, C. M. McPartlin, C. Whittingham, D. J. Williams and T. M. Woodroffe, *J. Organomet. Chem.*, 1998, **551**, 313.
- ² D. F. Fischer, A. Barakat, Z.-q. Xin, M. E. Weiss and R. Peters, *Chem. Eur. J.*, 2009, **15**, 8722.
- ³ T. Sammakia, H. A. Latham and D. R. Schaad, *J. Org. Chem.*, 1995, **60**, 10.
- ⁴ J. Tao, J. P. Perdew, V. N. Staroverov and G. E. Scuseria, *Phys. Rev. Lett.*, 2003, **91**, 146401.
- ⁵ S. Grimme, J. Antony, S. Ehrlich and H. Krieg, *J. Chem. Phys.*, 2010, **132**, 154104.
- ⁶ a) F. Mendizabal, S. Miranda-Rojas and L. Barrientos-Poblete, *Comput. Theor. Chem.*, 2015, **1057**, 74; b) Z. Qu, A. Hansen and S. Grimme, *J. Chem. Theory Comput.*, 2015, **11**, 1037; c) L. Nunes dos Santos Comprido, J. E. M. N. Klein, G. Knizia, J. Kästner and A. S. K. Hashmi, *Angew. Chem. Int. Ed.*, 2015, DOI: 10.1002/anie.201412401; d) P. Nava, D. Hagebaum-Reignier and S. Humbel, *ChemPhysChem*, 2012, **13**, 2090.
- ⁷ L. F. Paštka, T. Rajský and M. Urban, *J. Phys. Chem. A*, 2013, **117**, 4472.
- ⁸ J. P. Perdew, K. Burke and M. Ernzerhof, *Phys. Rev. Lett.*, 1996, **77**, 3865.
- ⁹ a) A. C. Tsipis, *Coord. Chem. Rev.*, 2014, **272**, 1; b) R. Kang, H. Chen, S. Shaik and J. Yao, *J. Chem. Theory Comput.*, 2011, **7**, 4002; c) G. Ciancaleoni, S. Rampino, D. Zuccaccia, F. Tarantelli, P. Belanzoni and L. Belpassi, *J. Chem. Theory Comput.*, 2014, **10**, 1021; d) M. Bühl, C. Reimann, D. A. Pantazis, T. Bredow and F. Neese, *J. Chem. Theory Comput.*, 2008, **4**, 1449; e) R. Kang, W. Lai, J. Yao, S. Shaik and H. Chen, *J. Chem. Theory Comput.*, 2012, **8**, 3119.
- ¹⁰ S. Grimme, J. Anthony, S. Ehrlich and H. Krieg, *J. Chem. Phys.*, 2010, **132**, 154104.
- ¹¹ G. Mazzone, N. Russo and E. Sicilia, *J. Chem. Theory Comput.*, 2015, **11**, 581.
- ¹² W. Kohn and L. J. Sham, *Phys. Rev.*, 1965, **140**, A1133.
- ¹³ G. Knizia, *J. Chem. Theory Comput.*, 2013, **9**, 4834.
- ¹⁴ P. G. Jones and J. Lautner, *Acta Cryst.*, 1988, **C44**, 2089.
- ¹⁵ a) F. Weigend, M. Häser, H. Patzelt and R. Ahlrichs, *Chem. Phys. Lett.*, 1998, **294**, 143; b) F. Weigend and R. Ahlrichs, *Phys. Chem. Chem. Phys.*, 2005, **7**, 3297.
- ¹⁶ M. Sierka, A. Hogekamp and R. Ahlrichs, *J. Chem. Phys.*, 2003, **118**, 9136.
- ¹⁷ a) R. Ahlrichs, M. Bär, M. Häser, H. Horn and C. Kölmel, *Chem. Phys. Lett.*, 1989, **162**, 165; b) TURBOMOLE V6.4 2012, TURBOMOLE GmbH.
- ¹⁸ A. Klamt and G. Schürmann, *J. Chem Soc., Perkin Trans. 2*, 1993, 799.
- ¹⁹ D. Andrae, U. Haussermann, M. Dolg, H. Stoll and H. Preuss, *Theor. Chim. Acta*, 1990, **77**, 123.
- ²⁰ E. F. Pettersen, T. D. Goddard, C. C. Huang, G. S. Couch, D. M. Greenblatt, E. C. Meng and T. E. Ferrin, *J. Comput. Chem.*, 2004, **25**, 1605.
- ²¹ A. A. Mohamed, H. E. Abdou and J. P. Fackler Jr., *Coord. Chem. Rev.*, 2010, **254**, 1253.
- ²² a) A. J. Atkins, M. Bauer and C. R. Jacob, *Phys. Chem. Chem. Phys.*, 2013, **15**, 8095; b) A. J. Atkins, C. R. Jacob and M. Bauer, *Chem. Eur. J.*, 2012, **18**, 7021; c) C. J. Ziegler, K. Chanawanno, A. Hasheminasab, Y. V. Zatsikha, E. Maligaspe and V. N. Nemykin, *Inorg. Chem.*, 2014, **53**, 4751.

-
- ²³ H. Koch, P. Jørgensen and T. Helgaker, *J. Chem. Phys.*, 1996, **104**, 9528.
- ²⁴ H.-J. Werner, P. J. Knowles, G. Knizia, F. R. Manby and M. Schütz, *WIREs Comput. Mol. Sci.*, 2012, **2**, 242.
- ²⁵ a) M. A. Celik, C. Dash, V. A. K. Adiraju, A. Das, M. Yousufuddin, G. Frenking and H. V. R. Dias, *Inorg. Chem.*, 2013, **52**, 729; b) L. Batiste and P. Chen, *J. Am. Chem. Soc.*, 2014, **136**, 9296; c) D. Marchione, L. Belpassi, G. Bistoni, A. Macchioni, F. Tarantelli and D. Zuccaccia, *Organometallics*, 2014, **33**, 4200. d) L. F. Paštěka, T. Rajský and M. Urban, *J. Phys. Chem. A*, 2013, **117**, 4472; e) A. Comas-Vives and J. N. Harvey, *Eur. J. Inorg. Chem.*, 2011, 5025.
- ²⁶ a) M. Chen, Y. Chen, N. Sun, J. Zhao, Y. Liu and Y. Li, *Angew. Chem. Int. Ed.*, 2015, **54**, 1200; b) C. Latouche, Y.-R. Lin, Y. Tobon, E. Furet, J.-Y. Saillard, C.-W. Liu and A. Boucekkine, *Phys. Chem. Chem. Phys.*, 2014, **16**, 25840; c) A. Comas-Vives and J. N. Harvey, *Eur. J. Inorg. Chem.*, 2011, 5025.
- ²⁷ G. Cui, X.-Y. Cao, W.-H. Fang, M. Dolg and W. Thiel, *Angew. Chem. Int. Ed.*, 2013, **52**, 10281.
- ²⁸ G. Knizia, *IboView*; see <http://www.iboview.org>.